3D Facial Skin Texture Analysis Using Geometric Descriptors

Seck, Alassane; Dee, Hannah Mary; Tiddeman, Bernie

Published in:
22nd International Conference on Pattern Recognition

DOI:
10.1109/ICPR.2014.203

Publication date:
2014

Citation for published version (APA):
Seck, A., Dee, H. M., & Tiddeman, B. (2014). 3D Facial Skin Texture Analysis Using Geometric Descriptors. In *22nd International Conference on Pattern Recognition* (pp. 1126 - 1131). (International Conference on Pattern Recognition). IEEE Press. https://doi.org/10.1109/ICPR.2014.203

3D Facial Skin Texture Analysis Using Geometric Descriptors

***Abstract*—We compare skin texture classification using various 2D texture descriptors and on the other hand, their extensions to 3D surface orientation data. We perform a multi-resolution analysis on both the 2D and 3D data. Rotation-Invariant Local Binary Patterns, Multiple Orientations Gabor Filters and Center-Symetric Autocorrelation are used to extract 2D texture features from high resolution facial skin albedo patches. For extracting texture feature directly from the corresponding normal map patches, we propose extensions of these texture measures in both the slant/tilt and tangent spaces. We compare the results of classifying facial wrinkles and pores using the 2D-based and 3D-based texture features. We use the 3DRFE dataset which consists of high resolution 3D facial scans along with the corresponding photometric and albedo images. We notice a net improvement on both classifying wrinkle and pore using the 3D orientation based features over the 2D ones.**

I. Introduction

Texture analysis is an important task in automated image processing and computer vision. It has been widely used in applications such as medical image processing, content-based image retrieval and face identification among others. However, it has been seen mostly as a 2D problem. In current studies, texture feature are generally extracted from 2D images, exploiting information such as color, brightness, contour etc. Although there is no unanimously accepted definition of surface texture, it is obvious that humans use relief and occlusion related information in the process of perceiving and discriminating texture. Psychological studies have supported that assertion. He and Nakayama, by manipulating binocular disparities of texture elements, conclude that the visual system cannot ignore information regarding surface layout in texture discrimination [9]. Ho and Maloney show that images formed under fixed lighting and viewing conditions convey only partial texture roughness information to human observers [10], [11].

In the Computer Science community, some studies have been interested in showing the relevancy of considering surface texture processing as a 3D problem. Sejong and Yoonsuck prove that texture segmentation is more effective and accurate in a 3-dimensional configuration [13]. In Computer Vision, several surface texture processing related works consider 3D informations. Smith *et al* propose a method for computing a co-occurrence matrix for normal maps [17]. Sandbach *et al* compute Local Binary Patterns on depth maps and APDIs (Azimuthal Projection Distance Image) of normal maps to classify 3D facial action units [16]. Peyre and Mallat propose a bandelets approach for compressing and characterizing 3D surface geometry.

The issue has also raised interest in the Skin Bioengineering community too. A number of studies have used 3D surface texture to analyse skin disruption. Warr *et al* demonstrate the considerable value added by augmenting the classical 2D ABCD features with 3D pattern analysis in classifying benign and malignant Melanoma [5]. Koh *et al* use a 3D imaging system to quantify skin surface roughness and acne volumes. Warr *et al* use first and second order differential forms of skin surface relief to describe skin lesion disruption.

This growing interest in 3D surface texture characterisation is also motivated by the increasing availability of high resolution 3D datasets due to the ceaseless advances in 3D surface capture and recovery techniques. Today, high resolution 3D surface reconstructions can be achieved with great precision. Multi-view stereo systems can reconstruct surface geometry with an accuracy of about a tenth of a millimetre [7] while laser-based systems can achieve a precision of up to a thousandth of a millimetre [4]. Structured Light (also known as Active Stereo) systems tends to outperform multi-view systems in precision and speed whereas Photometric Stereo techniques can generate surface orientations with a resolution that is only limited by the resolution of the sensor used to capture the images. Recent studies have combined the last two techniques to produce highly detailed 3D human facial datasets that holds information about to the skin fine structure (down to the level of the pores) [12], [18].

In this paper, we propose a comparative study of skin texture analysis using, on one hand various rotation-invariant 2-dimensional texture descriptors and on the other hand, their extensions to 3-dimensional surface texture. A multi-resolution scheme is adopted. Wrinkles and pores presence are classified on high resolution 3D facial scans. We also compare the 3D texture descriptors we propose to some others in the literature.

In the first section of this paper, we expose the motivations and the contributions of this work. In the second, we introduce the 2-dimensional texture descriptors we will experience with. In the third, we introduce our proposed extensions of these descriptors to 3-dimensional texture. And in the last section, we present and discuss our experimental results.

II. Motivation and Contributions

A. Motivation

A 2D image is a snapshot of a 3D scene with a set of well-defined conditions, including the lighting environment, the relative position of the camera and the objects forming the scene etc. These conditions together determine what is seen in the image and what is not. Thus a 2D image will not convey all the information present in the scene it represents and this is valid for the textures present in the scene. It is clear that some texture patterns can be totally captured and rendered in a 2D image without the above conditions considerably altering their appearance: a zebra skin macro-texture won't change

considerably on images with changes of lighting condition and viewpoint as long as there is enough ambient lighting. But, when it comes to textures with surface roughness as an areal image of a mountainous region or a bumpy unpolished wooden fabric, these imaging conditions can considerably affect their appearance in an image. Ho and Maloney studied the effects that lighting condition and view point can have on human perception of texture [10], [11].

In this, paper we are interested in skin texture and variations in appearance due to skin conditions. Despite the apparent global smoothness of its macro-structure, skin texture can be relatively rough in the meso and micro scales. Certain skin conditions such as wrinkles, lines, large pores, moles can even cause clearly visible surface irregularities on the skin. Therefore, skin texture does not escape from the issues stated above. We show in figure 1 how the apparent texture of a wrinkly skin region can change with lighting condition.

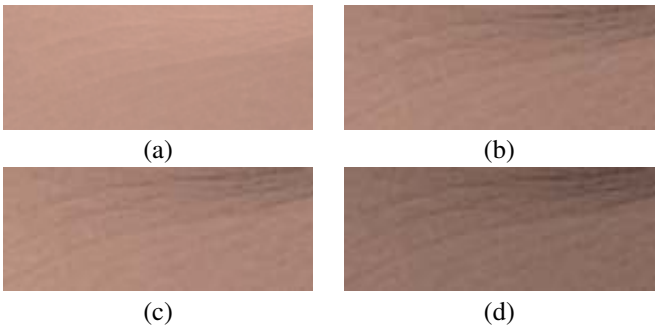

Fig. 1. Change of the apparent texture under different illumination conditions on a skin patch normal map. (a) light vector angle: 0 (b) light vector angle: $\frac{\pi}{4}$ (c) light vector angle: $\frac{\pi}{3}$ (d) light vector angle: $\frac{\pi}{2.2}$

It is clear that any 2D texture descriptor would give a different response to each of the images on figure 1 while they all represent the same skin patch. In addition, even if we assume that an image has been captured in optimal position and lighting conditions for best texture and roughness visibility, its 3D representation with the same resolution (which can be obtained with photometric stereo) will always hold more information about the surface texture. This is inherent to the process of recovering a 3D surface which involves change of lighting and/or viewing conditions. To illustrate this, we show in figure 2 the difference between applying a 2D Gabor filter to a skin patch diffuse and specular albedo (the latter being the 2D representation with the most surface detail) and our extension of Gabor filtering to 3D surface on the corresponding normal map (with same resolution as the albedos).

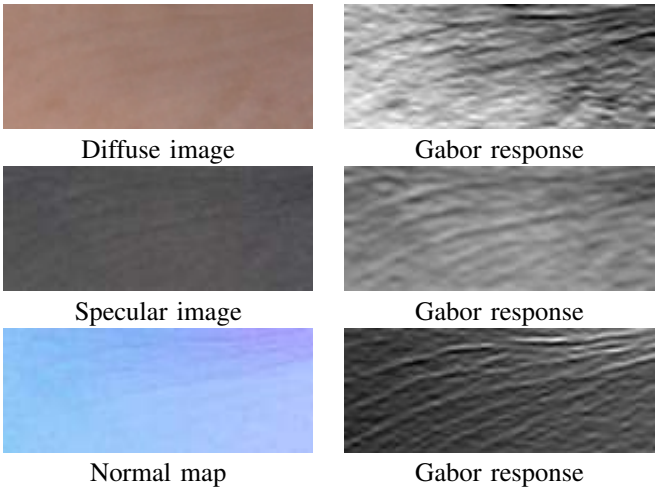

Fig. 2. Gabor responses from different representation of a wrinkly skin patch surface (The Gabor filter is set with an orientation of $\frac{\pi}{2}$, a standard deviation of 1.40 and a wavelength of 3. The images are 145×58)

These observations lead us to the conclusion that if it is technically possible to obtain 3D surface data with the same spatial resolutions as 2D images, we only can gain in analysing texture directly from the 3-dimensional data rather than from the 2-dimensional images, which are just partial representations of actual scene contents.

B. Contributions

We propose extended versions of Gabor filtering, Local Binary Patterns and Center-Symmetric Autocorrelation to surface orientation Data. We compare results of analysing skin texture using these proposed extensions on normal maps and their 2D counterpart on the corresponding albedo images. We also compare as well our 3D surface textures descriptors to some others recently proposed in the literature and show improved performance in classifying facial wrinkle and pore presence.

III. 2D TEXTURE DESCRIPTORS

We use multi-orientation and rotation invariant descriptors as most skin condition textures do not have a predominant orientation: a wrinkle is still a wrinkle, no matter if it appears vertical, oblique or horizontal on the face. We describe in this section three 2D texture descriptors which are Gabor Filter, Rotation-Invariant Local Binary Patterns and Centre-Symmetric Autocorrelation Function.

A. Gabor Filtering

Gabor filtering is widely used in texture segmentation [6], [1]. It has the advantage to approximate the two-dimensional receptive-field profiles of simple cells in the mammalian visual cortex [3]. The real part of a 2-dimensional Gabor Filter is represented by the function:

$$f(x, y, \sigma, \theta, \lambda, \gamma, \phi) = \exp\left(-\frac{x'^2 + \gamma^2 y'^2}{2\sigma^2}\right) \cos\left(2\pi \frac{x'}{\lambda} + \phi\right)$$

Which is a sinusoid enveloped in a Gaussian where $x' = x\cos\theta + ysin\theta$ and $y' = y\cos\theta - x\sin\theta$. σ, θ, λ, γ and

ϕ are respectively the Gaussian standard deviation, the filter orientation, the bandwidth, the aspect-ratio between the two axes and the phase.

In order to generate multi-orientation texture descriptors, a bank of Gabor filters has to be applied with different values of orientations. It is theoretically not possible to generate perfectly rotation-invariant descriptors, but more the bank of filters covers varied orientations, more the resulting descriptors are rotation robust. Figure 3 shows the Gabor responses with different orientations on a wrinkly skin patch.

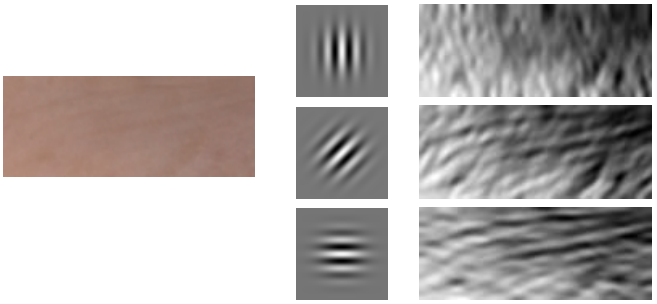

Fig. 3. Gabor responses for different orientations(respectively 0, $\frac{\pi}{3}$ and $\frac{\pi}{2}$) of a wrinkly skin patch surface (The Gabor filter is set with a standard deviation of 1.40 and a wavelength of 3. The images are 145×58)

B. Rotation-Invariant Local Binary Patterns

Local Binary Patterns are proposed by Ojala et al [14] as an extension of Texture Spectrum first introduced by Wang and He in the early nineties [19]. They are one of the most used texture measure method in the literature. They consist in thresholding, at any position, the neighbourhood to the central pixel and by multiplying the results by the corresponding binomial weight (Fig. 4).

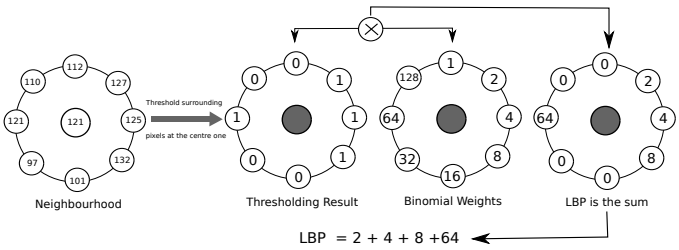

Fig. 4. Local Binary Patterns chart for an 8-pixels neighbourhood

In its original formulation, the Local Binary Patterns are not rotation-invariant. Ojala et al proposed a method of getting rotation-invariant Local Binary Patterns [15]. It consists in pre-computing a rotation-free dictionary of patterns, performing a circular shifting on each neighbourhood thresholding result till it matches one in the precomputed dictionary and finally assigning the corresponding index as the LBP value (Fig. 5). Figure 6 shows an example of Local Binary Patterns and Rotation-invariant Local Binary Patterns of a skin patch with acne.

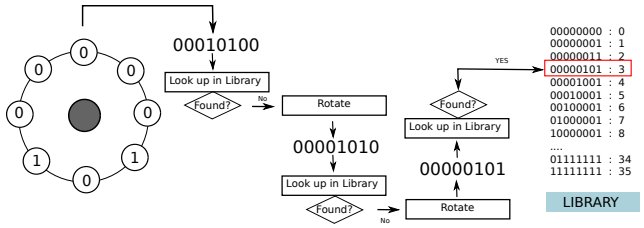

Fig. 5. Rotation-invariant Local Binary Patterns chart for an 8-pixels neighbourhood

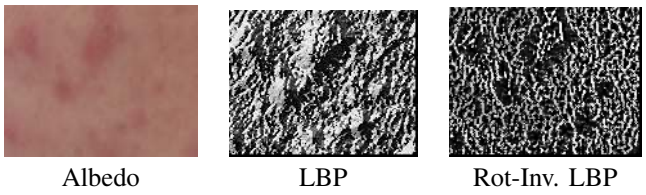

Fig. 6. LBP and Rotation-invariant LBP of an acne skin patch (8-pixel neighbourhood and radius 2)

C. Center-Symmetric Autocorrelation Function

Harwood et al proposed a set of Center-symmetric Auto-correlation related texture measures [8]. These measures include a linear and ranked center-symmetric auto-correlation (SAC and SRAC) and their corresponding covariance (SCOV). Because SCOV is not grey-level normalized, it holds more texture information than the SAC and SRAC. It is proven to outperform both SAC and SRAC in classifying 2-dimensional texture[8]. So we chose to experiment with SCOV in this work. Given a 8-pixels neighbourhood, the SCOV is given by the function in Fig. 7. In Fig. 8 we give an example of SCOV image of an acne skin patch.

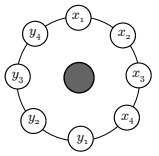

$$SCOV = \frac{1}{4}\sum_{i=1}^{4}(x_i - \mu)(y_i - \mu)$$

Fig. 7. Center-symmetric Covariance Function

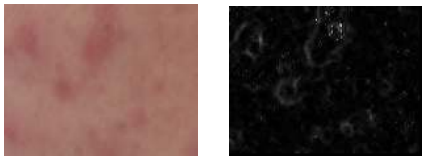

Fig. 8. SCOV image of an acne skin patch (radius 2)

IV. Analysing Texture using 3-dimensional Surface Orientation

We extend the three 2-dimensional texture measures presented in section III to analyse 3-dimensional orientation texture from dense normal maps. As a normal map is a classical RGB image where the red, green and blue channels encode respectively the X, Y and Z components of the normals, one

may consider applying directly 2-dimensional texture analysis algorithms to the normal maps. This would be theoretically inconsistent as unlike image pixels, normals do not satisfy the linearity condition required in the convolutions involved (a linear combination of two normals does not result in a unit-vector). Instead of calculating the texture measures introduced in section III directly on the normal maps, we propose deriving these from either the slant-tilt space or the tangent space.

a) Slant-Tilt space: The normal's slant and tilt are extracted at each position (Fig. 9). This results in a map where at each position we have two values corresponding to the normal's elevation and azimuth. For normalization sake, we keep the tangent values so the slant-tilt map is normalized in $[-1, 1]$. Considering $n = (n_x, n_y, n_z)$ denoting a normal, the slant and tilt tangent values are obtained with:

$$\tan\sigma = \frac{x^2 + y^2}{z} \quad , \quad \tan\tau = \frac{y}{x}$$

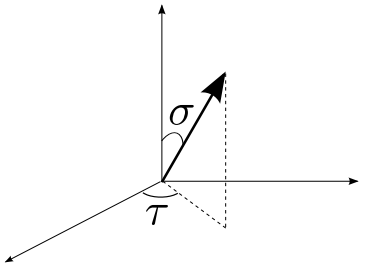

Fig. 9. A normal's Slant(σ) and Tilt(τ)

b) Tangent space: In this approach we consider the normals as elements of a Riemannian manifold and unfold these about the local means using a logarithm mapping (Fig. 10). This results in a tangent map whose elements are 2-dimensional coordinates and are obtained with:

$$\log_{\mu_{\theta_0,\tau_0}}(n_{\theta,\tau}) = \begin{cases} k\cos\theta\sin(\tau - \tau_0) \\ k(\cos\theta_0\sin\tau - \sin\theta_0\cos\theta\cos(\tau - \tau_0)) \end{cases}$$

With $\theta = \frac{\pi}{2} - \sigma$. θ_0 and τ_0 are the spherical coordinates of the local normal mean μ.

At each neighbourhood, the local normal mean is the one that minimises the mean of the geodesic distances to all the other normals in the same neighbourhood.

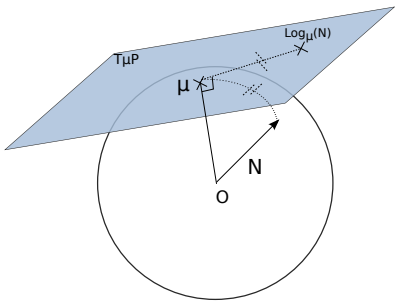

Fig. 10. Projection of a normal onto the local tangent plan

For visualisation purpose only, we compute single channel slant/tilt map and tangent map (figures 11 and 12). The pixel values are obtained with (for both the slant/tilt map and the tangent map):

$$I(i,j) = \arctan 2(y', x')\sqrt{x'^2 + y^2}$$

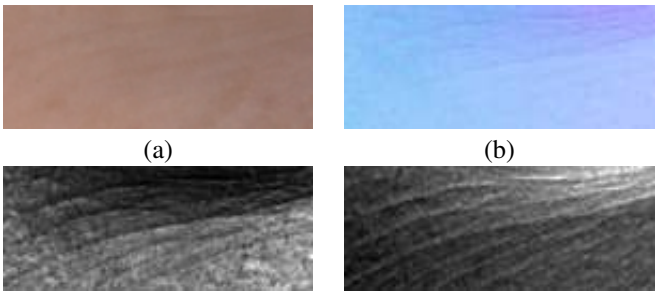

Fig. 11. Wrinkles patch - (a) Albedo(diffuse + specular), (b) Normal Map, (c) Slant/Tilt Map and (d) Tangent Map

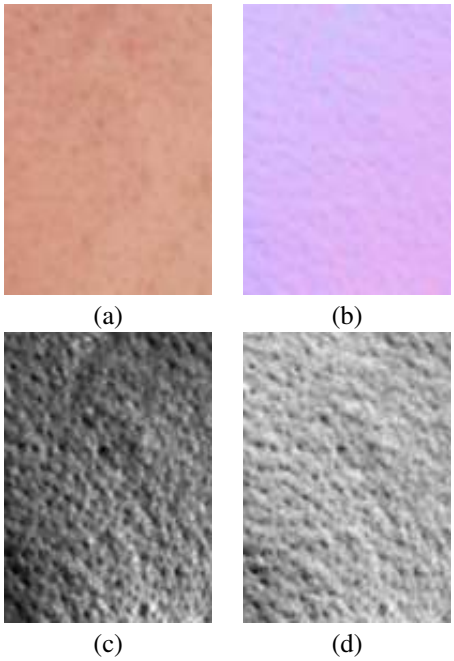

Fig. 12. Pores patch - (a) Albedo(diffuse + specular), (b) Normal Map, (c) Slant/Tilt Map and (d) Tangent Map

c) Analysis: We adopt a multi-scale scheme where at each level, the texture filter (one of those described in section III) is applied on either the slant-tilt map or the tangent map. This results in two responses, one for each channel. We normalize all the responses into the interval $[0, 1]$. Assuming $R^{c,l}$ denotes the response on the channel c at the level l, the normalization is performed with:

$$R^{c,l}_{normalized} = \frac{R^{c,l} - \min R^{c,l}}{\max R^{c,l} - \min R^{c,l}}$$

The histograms of the two normalized responses are computed and concatenated to form the texture descriptor at level

l. The same process is repeated at the subsequent level with a down-sampled version of the current normal map.

As we already illustrate, a convolution can not be done directly on the normals (because of these not being linear). So the down-sampling is done in the tangent plan with a Gaussian low pass, followed by projecting back the result in the original 3-dimensional space using the manifold exponential chart.

V. Experiments and Results

We have run a number of experiments to compare the responses of applying the different texture measures in 2D and 3D configurations and assess their effects on classifying facial skin conditions from high resolution albedo images and the corresponding normal maps. These experiments are preliminary as the dataset used (the ICT-3DRFE [18]) does not contain extensive skin condition variation. We are in the process of collecting our own skin condition dataset using the same class of 3D capture device used on the ICT-3DRFE dataset collection (a Lightstage [12]).

A. Ground Truth

We use the ICT-3DRFE dataset captured with a Lightstage. A Lightstage is a 3D capture device that combines photometric stereo techniques and multi-view (or structured light) techniques to produce high quality geometry and reflectance data. There are many advantages of using a Lightstage to capture facial skin condition dataset. First, the Lightstage is able to produce high quality mesh geometry and high resolution (down to the level of the pores) reflectance data (as normal maps). This not only provides us with adequate data to analyse fine skin texture, but also allows us to produce photo-realistic rendering of the skin, which is critical to the rating of the ground truth. Figure 13 gives an example of skin rendering we can achieve using rendering techniques described in Cook and Torrance 1982 [2].

Fig. 13. Our 3D Rendering of a face sample (zooming-in shows fine skin detail)

The second advantage is that the reflectance data produced by the Lightstage is given in different color channels. The provided normal maps are separated in to three diffuse (red, green and blue) and one specular channel. The diffuse normal maps' level of detail increases with the frequency. This means blue normal maps are more detailed than the green ones, which are in turn more detailed than the red ones. The specular normal map gives the most detailed structure of the skin surface. In this work we use the specular normal maps for 3-dimensional orientation data and an addition of the diffuse and specular albedo as 2-dimensional data.

Even though the ICT-3DRFE does not contain that much skin condition and ageing variation, we have managed to manually extract and rate in a scale of 4 levels (1 meaning "total absence" and 4 meaning "extremely visible") 31 patches visually judged wrinkly, 21 patches showing large pores and 30 smooth patches (for negative samples). Every patch is then divided in a number of fixed-size blocks (with 20% overlap). These blocks are used as individual samples for feature extraction.

We would like to consider a wider range of skin conditions, e.g. acne, moles, melanoma etc. However there is not enough presence of these conditions within the current dataset. We are taking this into consideration in the new dataset we are collecting.

B. Feature Extraction

For each sample, we build a 3-level multi-scale feature pyramid. The texture measures described in III are used on the albedo samples and their extensions described in IV are used on the normal map samples. We experiment a 3×3 and a 5×5 neighbourhoods for each of these texture measures. The feature pyramid size depends on the texture measure used and their parameter settings. We use a Support Vector Machine attribute evaluation to assign a rank to each of the features. In this work we chose to keep only the 256 best features regardless the texture measure used. The generated feature-vectors are used to train and test a 4 classes Multilayer Perceptron classifier.

C. Results and Comments

We summarize in tables I and II the results of classifying facial wrinkle and pore presence using 2D texture measures on skin patches albedo and their extensions to 3D surface orientation on the corresponding normal maps. We have implemented two other methods for texture analysis on normal maps recently proposed in the literature ([17], [16]) and compare these to our proposed extensions. We use a Leave-One-Out cross-validation strategy.

TABLE I. Results classifying wrinkles

		Recall		Precision		F-Measure	
		3×3	5×5	3×3	5×5	3×3	5×5
SAC	Albedo	0.56	0.58	0.50	0.55	0.52	0.56
	Slant-Tilt	0.80	0.82	0.82	0.82	0.81	0.82
	Tangent	0.78	0.80	0.81	0.82	0.79	0.81
RLBP	Albedo	0.54	0.56	0.52	0.51	0.53	0.53
	Slant-Tilt	0.78	0.80	0.78	0.79	0.78	0.79
	Tangent	0.78	0.81	0.76	0.77	0.77	0.78
Gabor	Albedo	0.59	0.62	0.61	0.62	0.60	0.62
	Slant-Tilt	0.83	0.87	0.84	0.0.86	0.83	0.86
	Tangent	0.85	0.90	0.86	0.89	0.85	0.89
Sandbach2012 (LABPs)		0.76	0.79	0.74	0.77	0.75	0.78
Smith2011		0.69		0.70		0.69	

TABLE II. RESULTS CLASSIFYING PORES

		Recall		Precision		F-Measure	
		3×3	5×5	3×3	5×5	3×3	5×5
SAC	Albedo	0.61	0.62	0.58	0.60	0.59	0.61
	Slant-Tilt	0.82	0.84	0.82	0.84	0.82	0.84
	Tangent	0.81	0.82	0.83	0.82	0.82	0.82
RLBP	Albedo	0.63	0.65	0.61	0.66	0.62	0.65
	Slant-Tilt	0.86	0.89	0.84	0.88	0.85	0.88
	Tangent	0.85	0.88	0.85	0.87	0.85	0.87
Gabor	Albedo	0.51	0.51	0.50	0.49	0.50	0.50
	Slant-Tilt	0.79	0.82	0.77	0.80	0.78	0.81
	Tangent	0.77	0.82	0.79	0.83	0.78	0.82
Sandbach2012 (LABPs)		0.78	0.80	0.77	0.79	0.77	0.79
Smith2011		0.70		0.69		0.69	

All three texture characterization methods used in this work show a clear improvement when used in a 3D configuration (slant/tilt or tangent space) on classifying both wrinkle and pore presence. The improvement is though less important in pore classification, which could be explained by the fact that pores are generally finer than wrinkles, so it is harder to get an accurate capture of their surface topology in a normal map.

The Gabor descriptors tend to give better results on classifying wrinkles whereas on classifying pores the Rotation-Invariant Local Binary Patterns appear to achieve better results.

Applying the texture measures on either the tangent or the slant/tilt space outperforms both the normal co-occurrence matrix proposed by Smith et al[17] and the LABPs(Local Azimuthal Binary Patterns) proposed by Sandbach2012 [16]. This is inherent of the lossy property of these two methods. In Smith's work a co-occurrence matrix is computed by sampling and indexing the slant/tilt range of values to generate a dictionary of slant/tilt - grey level pairs. Depending on the sampling factor, a number of normals with different orientation can be mapped to the same grey level. In Sandbach's work the projection of the normal map on the tangent map is used to generate a new image called Azimuthal Projection Distance Image(APDI). The APDIs pixels are obtained with the norm of the tangent coordinates which will be the same for all normals having the same slant.

VI. CONCLUSION

In this paper, we have investigated how an extra dimension could add value over classical 2D texture analysis methods, through an application to facial skin texture analysis. We have proposed small extensions of common 2D texture measures to 3D surface orientation data and conducted a comparative study between these. The results show considerable improvements on classifying facial wrinkle and pore presence when extracting the texture feature directly from the normal maps rather than from the corresponding albedo images. However it is clear that this improvement is tightly related to the nature of the texture analysed. If the texture is characterised by the surface roughness more than color or brightness information, geometric-based features would obviously be the best description choice. But if the surface intersect color variation is more determinant, radiometric information would describe the texture better than geometrical ones.

REFERENCES

[1] Jain A.K. and Farrokhnia F. . Unsupervised texture segmentation using Gabor filters . In *Systems, Man and Cybernetics, 1990. Conference Proceedings., IEEE International Conference on*, pages 14–19, 1990.

[2] Cook R.L. and Torrance K.E. A Reflectance Model for Computer Graphics. *ACM Trans. Graph.*, 1(1):7–24, January 1982.

[3] Daugman J.G. *Journal of the Optical Society of America A*, 2(7):1160–1169, Jul 1985.

[4] Digne J. and Audfray N. and Lartigue C. and Mehdi-Souzani C. and Morel J.M. Farman Institute 3D Point Sets - High Precision 3D Data Sets. *Image Processing On Line*, 2011, 2011.

[5] Ding Y., Smith L., Smith M., Sun J. and Warr R. Obtaining malignant melanoma indicators through statistical analysis of 3D skin surface disruptions. *Skin Research and Technology*, 15:262–270, 2009.

[6] Fogel I. and Sagi D. Gabor filters as texture discriminator. *Biological Cybernetics*, 61(2):103–113, June 1989.

[7] Furukawa Y. and Ponce J. Accurate, Dense, and Robust Multiview Stereopsis . *IEEE Transactions on Pattern Analysis and Machine Intelligence*, 32(8):1362–1376, 2010.

[8] Harwood D., Ojala T., Pietikäinen M., Kelman S. and Davis L. Texture classification by center-symmetric auto-correlation, using Kullback discrimination of distributions.

[9] He Z.J. and Nakayama k. Perceiving textures: Beyond filtering. *Vision Research*, 34(2):151–162, January 1994.

[10] Ho Y.X, Maloney L.T. and Landy M.S. How direction of illumination affects visually perceived surface roughness. *Journal of Vision*, 6:634–648, 2006.

[11] Ho Y.X, Maloney L.T. and Landy M.S. The effect of viewpoint on perceived visual roughness. *Journal of Vision*, 1:1–16, 2007.

[12] Ma W.C., Hawkins T., Peers P., Chabert C.F., Weiss M. and Debevec P. Rapid Acquisition of Specular and Diffuse Normal Maps from Polarized Spherical Gradient Illumination. In *Eurographics Symposium on Rendering*, 2007.

[13] Oh S. and Choe Y. Segmentation of Textures Defined on Flat vs. Layered Surfaces Using Neural Networks: Comparison of 2D vs. 3D Representations. *Neurocomput*, 70:13–15, August 2007.

[14] Ojala T. , Pietikäinen M. and Harwood D. A comparative study of texture measures with classification based on featured distributions. *Pattern Recognition*, 29(1):51–59, 1996.

[15] Pietikäinen M., Ojala T. and Xu Z. Rotation-invariant texture classification using feature distributions. *Pattern Recognition*, 33:43–52, 2000.

[16] Sandbach G., Zafeiriou S. and Pantic M. Binary Pattern Analysis for 3D Facial Action Unit Detection. In *Proceedings of the British Machine Vision Conference*, 2012.

[17] Smith M., Anwar S. and Smith L. 3D Texture Analysis using Co-occurrence Matrix Feature for Classification. In *Fourth York Doctoral Symposium on Computer Science*, 2011.

[18] Stratou G., Ghosh A., Debevec P. and Morency L. Effect of illumination on automatic expression recognition: A novel 3D relightable facial database . *IEEE International Conference onAutomatic Face & Gesture Recognition and Workshops*, pages 611–618, 2011.

[19] Wang L. and He D.C. Texture classification using texture spectrum. *Pattern Recognition*, 23:905–910, 1990.